Journal of Nondestructive Evaluation (2023) 42:8
https://doi.org/10.1007/s10921-022-00918-6

Use of Impedance Spectroscopy for the Characterization of the Microstructure of Alkali Activated SiMn Slag: Influence of Activator and Time Evolution

R. Navarro[1] · E. Zornoza[1] · E. G. Alcocel[2] · I. Sánchez[1]

Received: 13 September 2022 / Accepted: 3 December 2022

Abstract
The impedance spectroscopy technique has been used to study the microstructure of the binder resulting from the alkaline activation of SiMn slag. Two alkaline activators were used: waterglass and NaOH. Three different concentrations were analysed for both activators: 3.0, 3.5 and 4.0% Na_2O for NaOH; and 4.0, 4.5 and 5.0% Na_2O for waterglass with a constant SiO_2/Na_2O ratio of 1.0. The time evolution of the microstructure has been followed up using the non-destructive technique of impedance spectroscopy. This technique has been proved to be effective describing the microstructural changes in alkali activated pastes, and also can help predicting the mechanical behavior of mortars. The use of the resistivity itself seems to be deficient, but the analysis of the electrical parameters calculated from the impedance spectra measured gives a complete idea of the evolution in the material.

Keywords SiMn slag · Alkali activation · Pastes · Microstructure · Impedance spectroscopy

1 Introduction

It is a fact well known that the microstructure of materials in general, including cement based materials, is related to the service properties of the material [1, 2]. The understanding of the microstructure is essential to be able to modify the properties of the materials and select the most accurate cement or concrete for each use and environmental condition [3]. Cement based materials have a porous structure, that is mainly characterized by different techniques, such as mercury porosimetry, nitrogen absorption, water absorption and differential calorimetry [4]. All of these classical techniques are destructive and local. It means that a small sample of cement-based material is tested, and that sample must be discarded. Impedance spectroscopy has been proved to be an efficient non-destructive technique for following the development of the microstructure of porous materials such as the cement-based ones. It was initially used in the 1990s [5–7], but the results in the dielectric constant measured were not satisfactory. This fact was solved using the differential impedance analysis by Stoynov [8]. This tool showed the presence of two time constants in the high frequency arc, as it had been stated by some authors [9] without using the tool. The use of this technique allowed to understand the relation among electrical parameters from the equivalent circuit and elements of the microstructure for Portland cement [10], cements with additions [11–14], changes on the microstructure due to mechanical loading [15], cracking during service [16], chloride migration [17] or high temperatures [18, 19]. In the last years the technique has also been used on alkali activated materials. One of the first attempts tried to calculate the dielectric properties measuring in the frequency range from 1.0 MHz to 1.0 GHz, and studying the influence of the liquid content in the samples [20], but the aim of the work was not the characterization of the microstructure of the material. The same application of the impedance spectroscopy can be found in the study by Hanjitsuwan et al. [21]. Some other authors have used the electrochemical impedance spectroscopy to study the corrosion of reinforcements in alkali activated materials [22–25]. Other authors have used the technique in materials that include carbon additions [26, 27], and even it has been used for the following of mechanical loading and damage sensing [28]. After an exhaustive search in

✉ I. Sánchez
isidro.sanchez@ua.es

[1] Department of Civil Engineering, University of Alicante, Alicante, Spain

[2] Department of Architectonic Constructions, University of Alicante, Alicante, Spain

Published online: 13 December 2022

the literature, only one recent paper has been found about the use of impedance spectroscopy to study the evolution of the microstructure of alkali activated slag [29]. This paper studies up to 28 days of age the evolution of the electrical parameters in the range from 40 Hz to 35 MHz. The equivalent circuit used for the fitting is very similar to one proposed previously, that will be used in this work as well [10]. In the paper by Hu [29] there is also a very interesting study of the concentrations of different ions in the interstitial solution, and the evolution of these concentrations with time, and a deep study of the evolution of the resistances and characteristic frequencies of the impedance spectra, showing the capacity of the technique for following the evolution of the microstructure of alkali activated slags.

In this paper the development of the microstructure of an alkali-activated material has been studied. The precursor used is SiMg slag and two different activating dissolutions have been used, sodium hydroxide and waterglass. For this particular system some previous researches have been conducted in which the optimization of the mixtures was done [30], the mechanical properties of mortars using different types of fine aggregate were tested [31], and the microsctructure was studied using different classical destructive techniques (X-ray diffraction, thermogravimetry, and SEM [32]. The results obtained with these techniques do not allow to predict the mechanical behavior of the material presented in [31]. In the present research impedance spectroscopy has been used as the main technique for the study of the microstructure of the different alkali-activated materials. Since the technique monitors the bulk material (covers a big portion of the material), and non-destructive, the time of study has been extended up to 6 months from the preparation of the samples, so the evolution of microstructure is better analyzed in comparison to destructive techniques. Mercury porosimetry has been used as a contrast technique. In the present research, the activated material (ground granulated SiMn slag) is different to the slag studied in [29], where a blast furnace slag was used. The capacitances, which have been proved very important for the study of the microstructure of porous materials [18, 33, 34], are included in this paper as well, for a better understanding of the evolution of the microstructure of these materials, as a function of the activator, and sodium oxide content.

In the recently published paper [32] no significant differences were found among the use of any of the two activators, but the mechanical resistance reported in [31] showed higher resistance with time, and also as the % Na_2O increased. It was also proven that the best results for the compressive and flexural strength were obtained with waterglass as activator. So the origin of the different behavior due to the sodium oxide content and activator selected cannot be justified with the techniques used in [32], even though a good microstructural characterization was done. In this paper mercury intrusion porosimetry (MIP) and impedance spectroscopy have been used to complete the characterization of the microstructure. MIP shows some behaviors, like increasing tendencies with time for some cases (especially with waterglass as activator), while the compressive strength always increases. The use of impedance spectroscopy has two main advantages: first one is the big advantage of being non-destructive, fact that allows a continuous following of the same specimens. The second one is that it gives a global measurement of the material, since the measured area is a circle of 10 cm diameter, including all that volume of material in the measurement. As the results of this paper show, it can be used to predict the mechanical properties of the alkali activated slag. The values of the resistance show a continuous increasing tendency, even though the porosity decreases, and that is due to the continuous formation of solid products. The formation of solids is confirmed by the tendency found for the capacitance C_2. In addition to that result, the evolution of the electrical parameters has allowed the authors to propose a mechanism of development of the solid structure, that is coincident with a mechanism proposed for other alkali -activated materials.

2 Experimental

2.1 Raw Materials

A Spanish SiMn granulated slag supplied by Ferroatlántica plant placed at Boo-de-Guarnizo (Cantabria, Spain) was used. SiMn slag has a vitreous content of 96.0 ± 1.5% [30].

The determination of reactive silica (33.80%) and insoluble residue (3.35%) of the SiMn slag was made according to standards UNE 80225-2012 and UNE-EN 196-2-2014 [35, 36]. The original SiMn granulated slag was ground prior to use. The resulting slag has a fineness of 5512 cm^2/g [30]. The particle size range of slag was 0.32–113.58 μm, with a $D_{V,50} = 9.2$ μm and a $D_{4,3} = 15.2$ μm. The density of this SiMn slag is 2.916 g/cm^3 [37].

Alkaline solutions used to activate the SiMn slag were waterglass (WG) prepared with a commercial sodium silicate (Na_2SiO_3 (neutral solution QP, Panreac): SiO_2/Na_2O molar ratio = 3.28) and sodium hydroxide (NaOH) (technical grade, Panreac). Two different types of activators and three different activator concentrations have been tested: NaOH solution with a 3.0%, 3.5% and 4.0% of Na_2O; and a waterglass solution with a 4.0%, 4.5% and 5.0% of Na_2O. NaOH activating solutions was prepared by solving the required amount of sodium hydroxide in distilled water. WG solution was fabricated by mixing sodium silicate and sodium hydroxide in the appropriate quantities and the subsequent dilution of the mix with distilled water. The SiO_2/Na_2O ratio of the WG solution was set to 1.00. For the WG activator and the NaOH activator, a solution/slag ratio of 0.375 and 0.35 were used, respectively. These activating solutions were selected

according to the particular findings of a previous research [30, 31, 38].

2.2 Preparation of Slag Pastes

All pastes were prepared by the mixing of 1800 g of ground granulated SiMn slag and the calculated quantity of alkaline solutions, in a mixer Controls Automix (model 65-L0006/A) according to the standard UNE EN 196–3 [39]. All specimens have been cured in a humid chamber with a 100% of relative humidity (RH) and 20 ± 2 °C for all the duration of the study.

2.3 Analysis Techniques

2.3.1 Mercury Intrusion Porosimetry

The pore size distribution was obtained on paste by mercury intrusion porosimetry (MIP). Porosity measurements were conducted using an Autopore IV 9500 Micromeritics mercury porosimeter. Prior to analysis, the samples were conditioned at 60 °C for 12 h. The mercury pressure range for the equipment is 0.1 psi to 60,000 psi (0.0007–414 MPa), which implies that the equipment is capable of detecting pore diameter from 300 to 0.004 μm.

2.3.2 Impedance Spectroscopy

To perform this test, cylindrical moulds with a diameter of 10 cm were used and were filled with each of the analysed pastes. The samples were cured in a 100% RH environment for all the duration of the study, at 20 ± 2 °C. After demoulding the specimens, they were cut for obtaining cylinders 1 cm thick. The equipment used to perform the impedance test was an Agilent 4294 Impedance Gain/Phase analyser. The equipment has a maximum resolution of 10^{-15} F, and can measure from 10^{-14} to 0.1 F. The spectra were taken in the 100 Hz to 100 MHz range. Each paste was measured using two different settings that have already been used [10]. In the first configuration, the sample is in contact with two electrodes, and in the second configuration, the sample is not in contact with the electrodes and a polymer sheet is placed between them. The test conditions for both measurements were the same. In measurements where there is no direct contact between the sample and the two electrodes, to minimize fringing effects, the impedance value corresponding to the insulating polymer is subtracted from the value of the overall impedance by simple subtraction of complex numbers.

The impedance spectra measured were validated using Kramers–Kronig relationships to ensure the linearity, causality, and stability of the measurement [40]. Figure 1 shows the validity of measurements of samples prepared with 3.0% NaOH as activator at the age of 95 days, using both the configurations of contact and insulation among sample and electrode.

After validation of the measured data, and prior to the proposal of an electric circuit, the differential impedance analysis (DIA) [41, 42] was performed on the measured spectra, to determine the number of time constants. The number of time constants present determines the structure of the equivalent circuit. The results for the same data presented on Fig. 1 are depicted on Fig. 2.

As it can be seen on Fig. 2 with independence of the configuration, the number of time constants is 2 for the material. This means that the circuit that has already been proposed for cement-based materials, and widely used, can be initially used for the fitting of the spectra measured. These results are independent of the activator used, the concentration and the curing age.

The electrical data are calculated by fitting the experimental results to the proposed equivalent circuit. The use of this circuit is justified by the presence of two time constants on the impedance spectra of the materials. Both electrical circuits proposed for each of the configurations used, as well as the obtaining of the different electrical parameters were previously described [10] and used for different materials and conditions of the material [13, 17, 43].

2.3.3 Thermogravimetric Analysis

TGA was performed between 25 and 1100 °C at a heating rate of 10 °C/min in N_2 atmosphere (100 ml/min) in a Mettler Toledo TGA/DSC2.

3 Results and Discussion

3.1 Evolution of Microstructure Based on Porosimetry Analysis

As it is well known, the paste is the main responsible for the microstructure of the construction material. In previous works [30, 31] the porosity of mortars had been tested, but the porosity of the paste without aggregate has not been tested yet. Since the impedance spectroscopy has been done on paste samples, due to the reason above mentioned, it is necessary to obtain the mercury porosimetry of the materials.

Not only the total porosity and the pore size distributions have been measured. The mercury retained in the samples, after the test is finished, is representative of the development of the pore network, and of the tortuosity of the network as well, that is related to the pore network structure.

The data of total porosity are shown on Fig. 3, including the contribution of the different sizes of pore diameter, by decade, and the data of mercury retained after the tests are

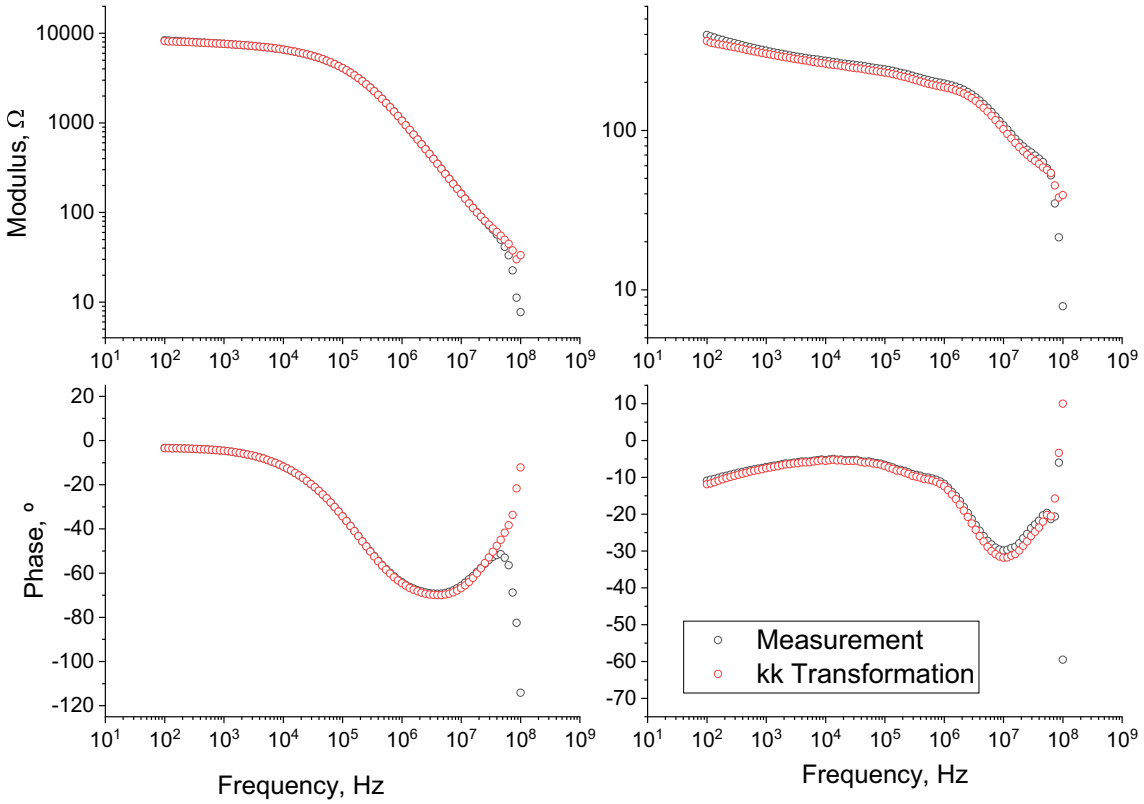

Fig. 1 Measured data and Kramers–Kronig calculation for a sample prepared with 3.0% of NaOH as activator and cured for 95 days in a humid chamber. The left figure depicts the validation of the data with contact electrode-material, while the right-side figure shows the validation of the data obtained with insulation on the interface

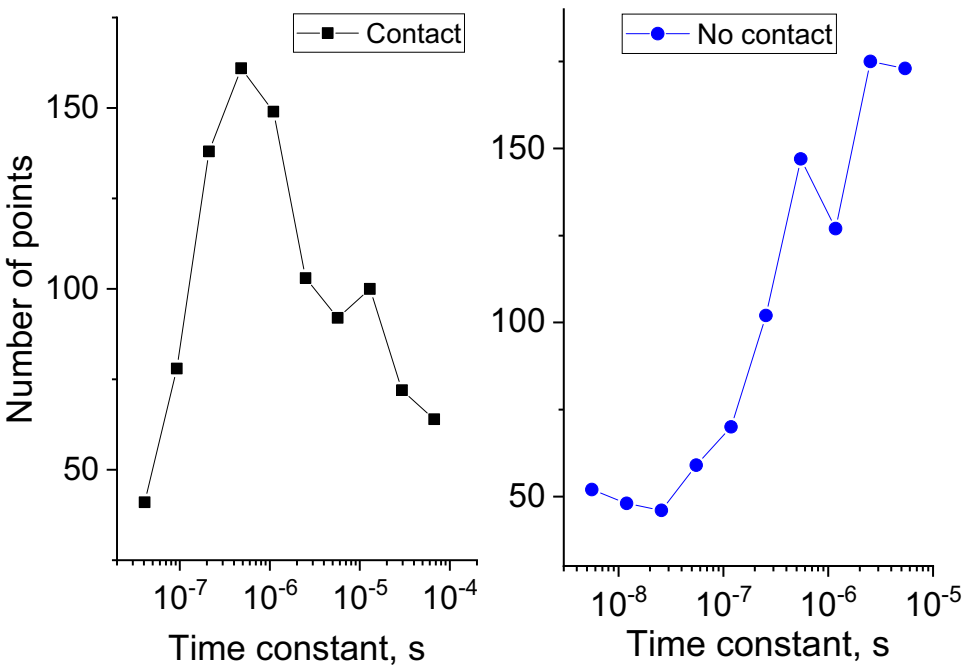

Fig. 2 DIA analysis of a sample activated with 3.0% NaOH cured for 95 days, with contact electrode-samples (left) and with insulation (right)

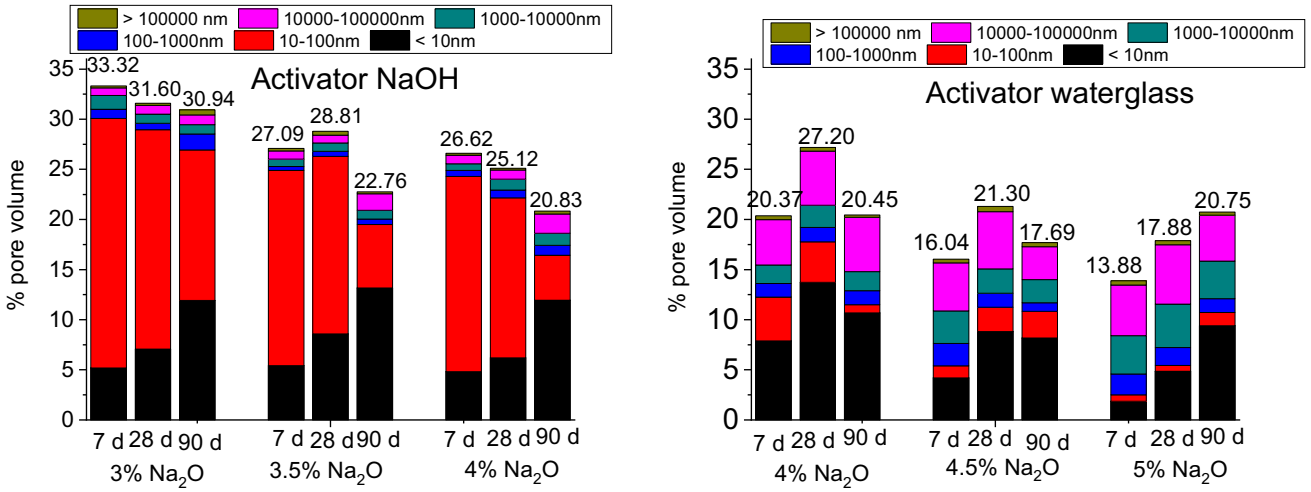

Fig. 3 Total porosity and pore size distribution per decades

Table 1 Percentage of mercury retained in the samples as a function of the activator used and of the sodium oxide content in the solution, and age

Activator	NaOH			Waterglass		
% Na_2O	3.0	3.5	4.0	4.0	4.5	5.0
7 days	64.00	71.70	69.65	73.68	79.75	83.87
28 days	63.93	68.08	73.25	68.04	77.64	82.24
90 days	54.44	69.61	75.31	81.07	74.01	76.42

shown on Table 1, as a function of the activator used and of the sodium oxide content in the solution.

As it could be expected from the results of the mortars already published, the value of the porosity generated using NaOH is always higher than the porosity obtained activating the slag with waterglass [31]. The value of the total porosity also decreases with time, as could be expected from previous results [31] and the results obtained using other alkali activated materials [29]. The samples activated with waterglass, show an increase at the age of 28 days, and the final porosity is similar to the value at 7 days, excepting for the activating solution with 5.0% of Na_2O, for which the value of the total porosity increases with time. This fact might have to do with the important expansion observed in samples that created visible cracks, bigger for the highest Na_2O concentrations, as it was reported in [30], and for a different precursor in [44]. The possibility of cracking by expansion is also confirmed by the lower mercury retained which decreases with time, a fact that might be due to the crack opening that makes easier the exit of mercury from the pores after intrusion. Usually, the increase of small pores with time causes a reduction of big diameter pores. That behaviour has been widely reported [3, 12, 13]. In this work the behavior is quite different. In this case, the fraction of big pores increases even though the total porosity decreases, as it can be seen on Fig. 3. For example, the case of using NaOH as activator, with a Na2O concentration of 3%. This increase of the pores of diameter above 10 μm cannot be attributed to the reactions in the alkali activated material, because it is solid after 1 day. The only reason could be the formation of cracks, due to expansion or shrinkage. The fraction of pores with diameter smaller than 100 nm increases with time significantly, indicating progress in the reaction and microstructure development. In the case of using waterglass as activator, paying attention to Fig. 3 it can be seen that, for example the case of using a 5% of Na2O, the volume of small pores increases in an important way, but the volume occupied by bigger pores increases from 7 to 28 days, and remains more or less constant from 28 to 90 days. It clearly means that the small pores come from the formation of solid products within the bigger pores, but also new pores of big size are being formed, to increase the volume of bigger pores, or maintain it constant, and it can only be due to the formation of cracks. The expansive behavior in early ages was already described in recent works in the field [45, 46]. With independence of the activator the formation of cracks, that increase the volume of pores with diameter higher than 10 μm is confirmed by the decrease of the retained mercury fraction within the pores, because the cracking increases the accessibility of mercury to pores.

Figure 4 shows the appearance of samples activated with different concentrations of NaOH and WG activators. Samples with waterglass and 5.0% Na_2O showed visible

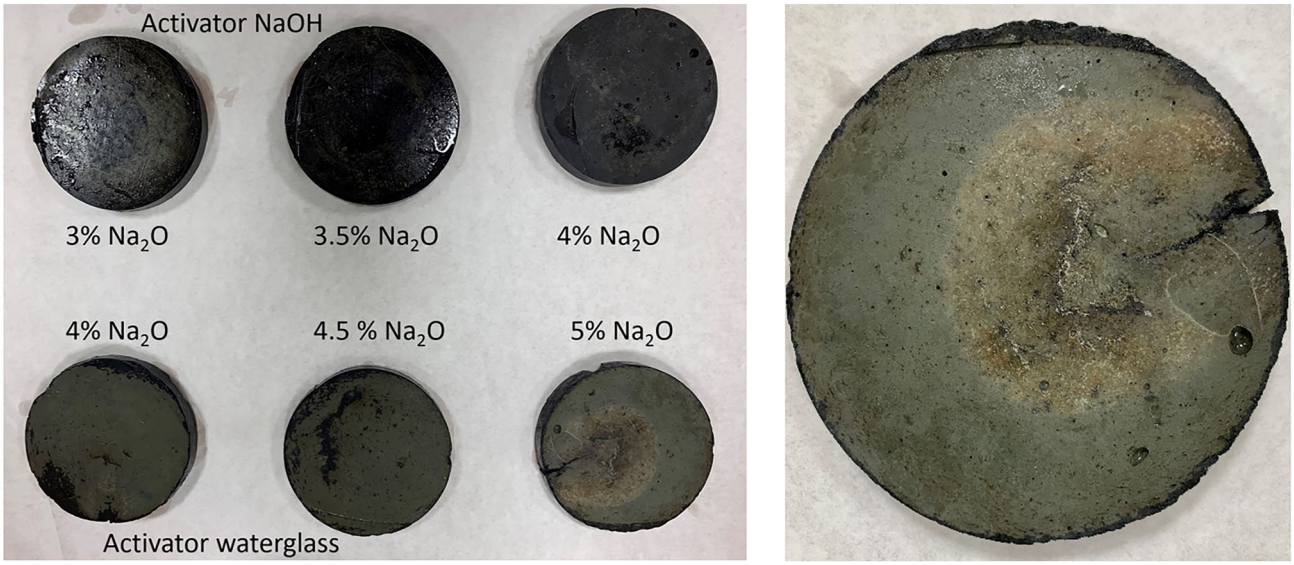

Fig. 4 Aspect of the samples as a function of activator and sodium oxide content. The picture on the right is an enlargement of the sample activated with WG and 5.0% of Na_2O

macrocracks due to expansion. The value of mercury retained does not show a clear tendency, but in most cases, it seems to decrease.

The analysis of the pores by size is shown in Fig. 5. As it can be easily observed, there is a clear evolution with time that makes decrease the fraction of coarse pores and a clear increase of the pores with size smaller than 10 nm. It has to be pointed out that the equipment used has a lower limit of detection of 4 nm, and the curves of pore size distributions suggest the presence of more pores in the region where pores cannot be measured. This fact will imply almost no change in total porosity, because pores are very small, but they will affect the electrical factors in a very important way.

It is clear the decrease of the pore dimensions, and the last family of pores cannot be measured due to the equipment limitations, especially for samples where waterglass was used as activator.

3.2 Evolution of Microstructure Based on Impedance Spectroscopy Analysis

As it was stated in the experimental section, due to the presence of two time constants and the nature of the pastes prepared, the equivalent circuits, shown on Fig. 6, used for the fitting of the impedance spectra obtained can be those reported in [10]. The association of the parameters present in the different circuits was widely described in [33]. As it is described there, an proven by experimental results and simulation the capacitance C_1 represents the solid fraction of the porous material, and the higher is the value of C_1 the lower is the porosity of the sample. C_2 represents the interface solid-electrolyte in porous materials. So, somehow this capacitance is a measurement of the internal surface of the pores, since the cement based materials are so hydrophilic that they keep a thin layer of contact solid-electrolyte even in extremely dry cement based materials [18].The resistances R_1 and R_2 represent the resistance of the pores. R_1 represents the resistance of the pores that electrically connect both sides of the sample studied, while R_2 represents the pores that do not allow electrical connection among both sides of the sample. In case of non-contacting measurements R_2 represents all the pores connected in parallel. The value of the resistance R_1, associated to the connecting pores, can only be obtained from the measurements where sample and electrodes are in contact, while the rest of the parameters be obtained both from the contacting and non-contacting measurements. The results of the resistance R_1 were obtained from the first configuration, and the values of the resistance are shown on Fig. 7.

As it has already been said, this resistance is associated to the crossing pores. As it can be clearly seen, and as it could be expected from the mercury porosimetry results, the value of the resistance has an increasing tendency with time, as the porosity decreased. The value of the resistance depends not only on the total porosity, but on the pore size distribution. Samples where sodium hydroxide was used as activator show a continuous increasing tendency on the resistance, and even though the values of the porosity are smaller for samples with 4.0% Na_2O, the bigger percentage of big pores, mainly in the range from 10,000 to 100,000 nm of the samples with higher sodium oxide contents, compensate the total porosity. The other aspects that influence the behavior of the resistances in cement-based materials are the conductivity of the electrolyte and the saturation degree. A recent paper, that activates another type of slag using waterglass, has proved

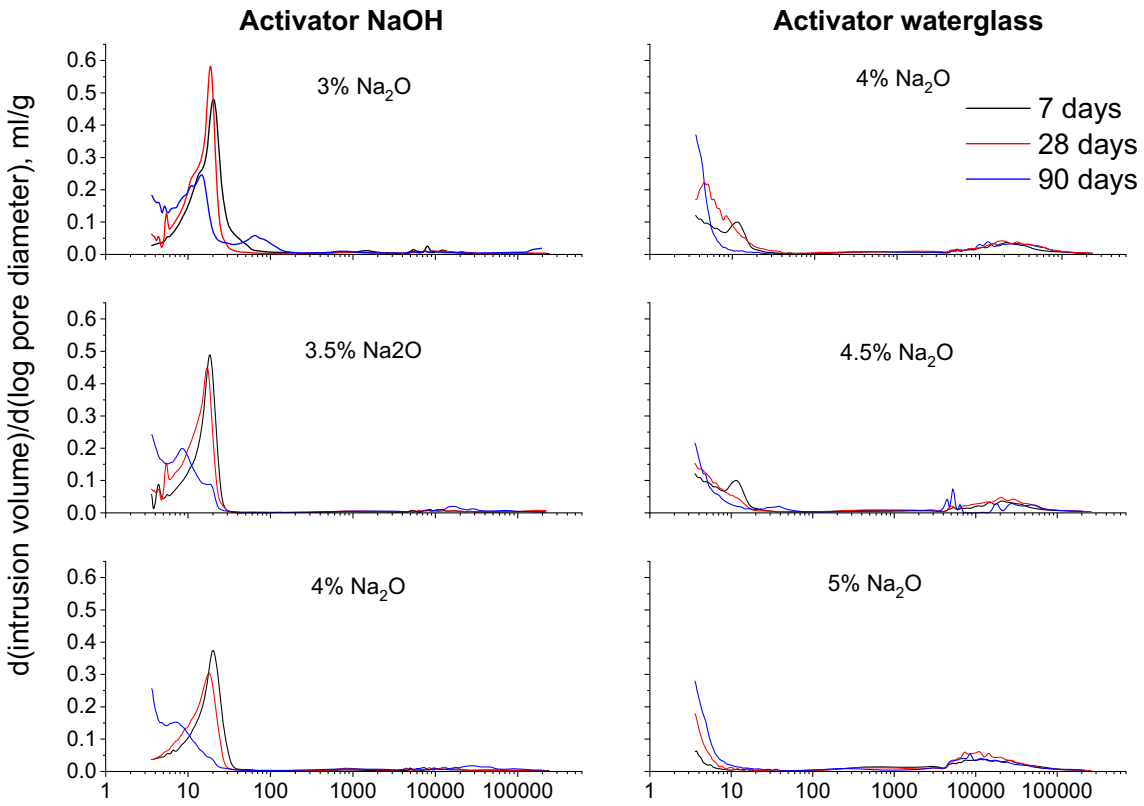

Fig. 5 Pore size distribution in the samples as a function of the activator used, the sodium oxide content in the solution, and age

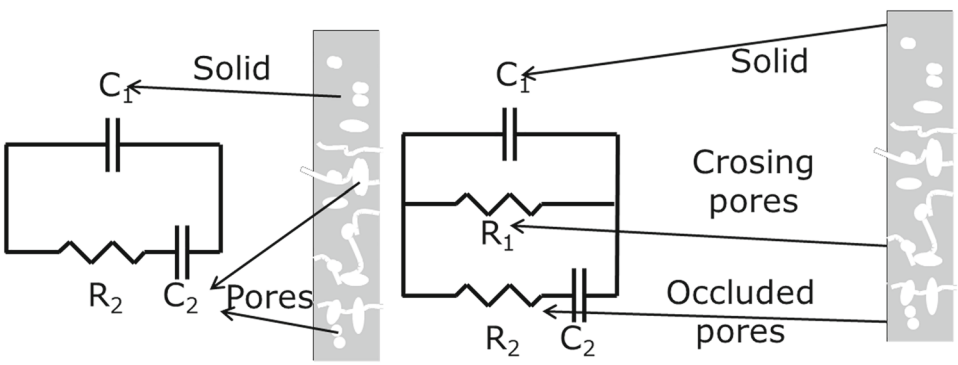

Fig. 6 Equivalent circuits used for the fitting of the measured impedance spectra using the non-contacting method (left) or contacting method (right) (from [10])

that the concentration of the main ions in the solution remains approximately constant after 10 days, with independence of the Na_2O concentration, and that it is influenced by the initial concentration of each ion in the activating solution [29]. According to this result, the conductivity of the pore electrolyte should be proportional to the initial solutions used for the activation of the precursor. The conductivity of the activating solutions is shown in Table 2. The value of the conductivity is higher for the samples that were activated with NaOH, but they show the higher resistance, that could be due to a higher ionic consumption during the activation reactions or only to the difference in pore dimensions.

The mass of each sample was measured during the process, and the average mass gains for each sample are shown on Fig. 8. As it can be observed, there is an increase in the mass for every set of samples, but the value of mass gained is higher for the samples activated with waterglass. The behavior of mass gain has already been described [44], and in that case the increase of mass was lower for the samples with higher sodium oxide content. This means that all the pores in the sample would possibly be water saturated. This could be expected since the samples were kept in a hermetic container with distilled water in the bottom, avoiding contact with the samples. The higher increase was measured in the samples hydrated with waterglass, in coincidence with the big pores

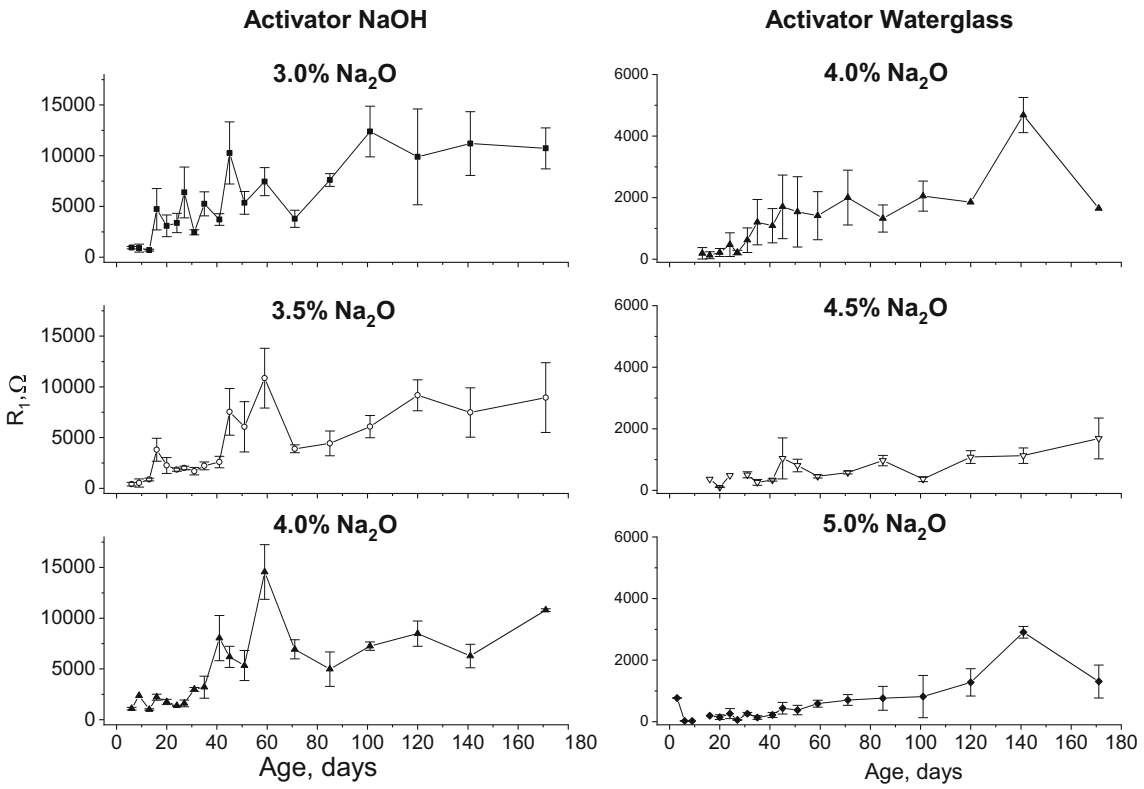

Fig. 7 Time evolution of the resistance R_1 as a function of activator and sodium oxide content

Table 2 Solution conductivity as a function of activator and sodium oxide content

Activator NaOH		Activator waterglass	
% Na_2O	Conductivity (mS)	% Na_2O	Conductivity (mS)
3.0	363	4.0	129.6
3.5	382	4.5	121.1
4.0	396	5.0	110.4

detected, that in case of no saturation would be the first ones to dry. So, after all this analysis it seems clear that the lower value of the resistances measured in the samples is due to the presence of pores with size among 10,000 and 100,000 nm. These big pores would not be interconnected through small pores, fact that will cause an increase in the resistance, but they seem to be in parallel with those small pores, being the dominant ones in the measured resistance. The increasing tendency of the resistance would be due to the decrease in the fraction of big pores that, due to the continuous reaction, shows an evolution towards smaller pores.

If the samples activated with the same activator type and different sodium oxide contents are compared, it can be seen that all of them show similar values. For the case of NaOH as activator, the highest value is shown by the samples with lower Na_2O content, mainly in the long term. This sample shows the lowest percentage of pores below 10 nm, and similar percentages of pores among 10 and 1000 nm, and the highest porosity. However, this could be compensated by the lowest conductivity of the interstitial solution, since the activating solution was the one with the lowest conductivity. For the case of waterglass as activator, the highest value of the resistance R_1 is presented by the samples with 4.0% Na_2O. It must be pointed out here that these samples did not show visible cracks, and this could be one of the determining facts in the resistive behavior of the material. Moreover, samples with 4.0% of sodium oxide presented similar porosity values after 90 days than the rest of the samples and always the highest content of pores with size smaller than 10 nm, and similar or smaller percentages of pores above 10,000 nm. Similar results were reported on [29], with an increasing tendency of the resistance with time and a decreasing tendency with the percentage of Na_2O, also in coincidence with the porosimetry results, but not in deep discussion was made about this fact. Some other papers study the resistivity of the alkali activated materials for self-sensing, but not evolution or dependence on activator is presented [27].

So, it can be concluded, that even though many authors use the resistivity of the samples to measure microstructure-related properties of the samples the different contributions of the different facts (porosity and pore size distribution, water

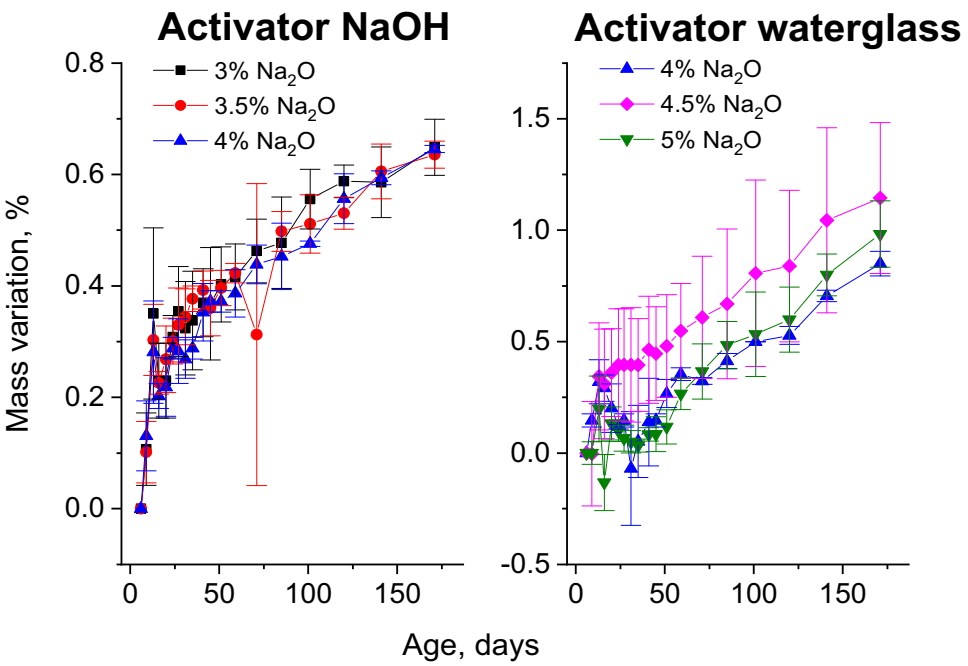

Fig. 8 Average mass variation for the samples activated with time

saturation, conductivity, and shrinkage) make this parameter itself not suitable for following the microstructure evolution in alkali-activated materials.

Regarding the resistance R_2, it is obtained from the non-contacting measurements due to the higher precision in determining this parameter as has been widely reported [15, 43]. The behavior of this resistance is very similar to the evolution exhibited by the resistance R_1, and the explanation could be the same for every parameter, since this parameter is also associated to the pores resistivity and the factors that influence the resistivity of the pores do not change with the impedance spectra measurement setup. The evolution of the values of resistance R_2 is show on Fig. 9.

The values of the capacitance C_2 are associated to the surface in contact solid-electrolyte so, they have been shown to be a good parameter to follow the development of the reactions [11, 12, 47], whatever the origin of the changes in the microstructure is. The values for the capacitance C_2 obtained from the fitting of the measurements obtained avoiding contact among alkali-activated material and electrode are shown on Fig. 10. These measurements have the highest precision for the calculation of the value of this parameter.

The values for the capacitance C_2 for samples activated with NaOH show a clear decreasing tendency among 10 and 50 days, and then they show a slightly increasing tendency, that continues with time. The values of the capacity for all sodium oxide contents are very similar, showing samples with 4.0% Na_2O a clearer increasing tendency from 60 days to the end of the measurement campaign. Both resistances, R_1 and R_2 showed an almost constant increasing tendency. Taking both data, resistances and capacitance C_2, the way the microstructure evolves with time could be the following: the initial microstructure of the materials was quite irregular in the first days. The irregular surface will mean a big contact surface solid-electrolyte, and therefore, a high value for C_2. Due to the reaction progress, higher solid amount will be formed, and the pore surface could adopt a more regular shape due to the deposition of the new solids over the pore walls. This could cause a decrease of the surface of contact electrolyte-solid, between 10 and 50 days. This decrease of the contact surface will imply a decrease of the value of the capacitance C_2. After 50 days the continuous formation of solids will continue, as suggested by the continuous growing tendency of the resistances. The solids formed after that age, will be formed on a quite smooth surface (formed up to 50 days) and the new solids will again increase the surface of contact, and therefore the value of C_2, but the increase is slighter than the decrease, possibly due to the lower amount of solids formed at this ages. A schematic representation of the growing process, according to these results is depicted on Fig. 11. A two-step mechanism similar to the described here has been reported in [48]. This behavior could not have been predicted from the resistance measurements, possibly due to the coexistence of pores that are being closed while others have not started the filling yet, and that could be the reason why the values of the resistance show a continuous increase. This result is in coincidence with the time-evolution of the porosity for samples with 3.0% of NaOH, that shows a more important decrease among 7 and 28 days, and then the porosity does not decrease that fast, but for the rest of the samples the behavior has nothing to do with that. The refinement of the pores is also more important between 28 and

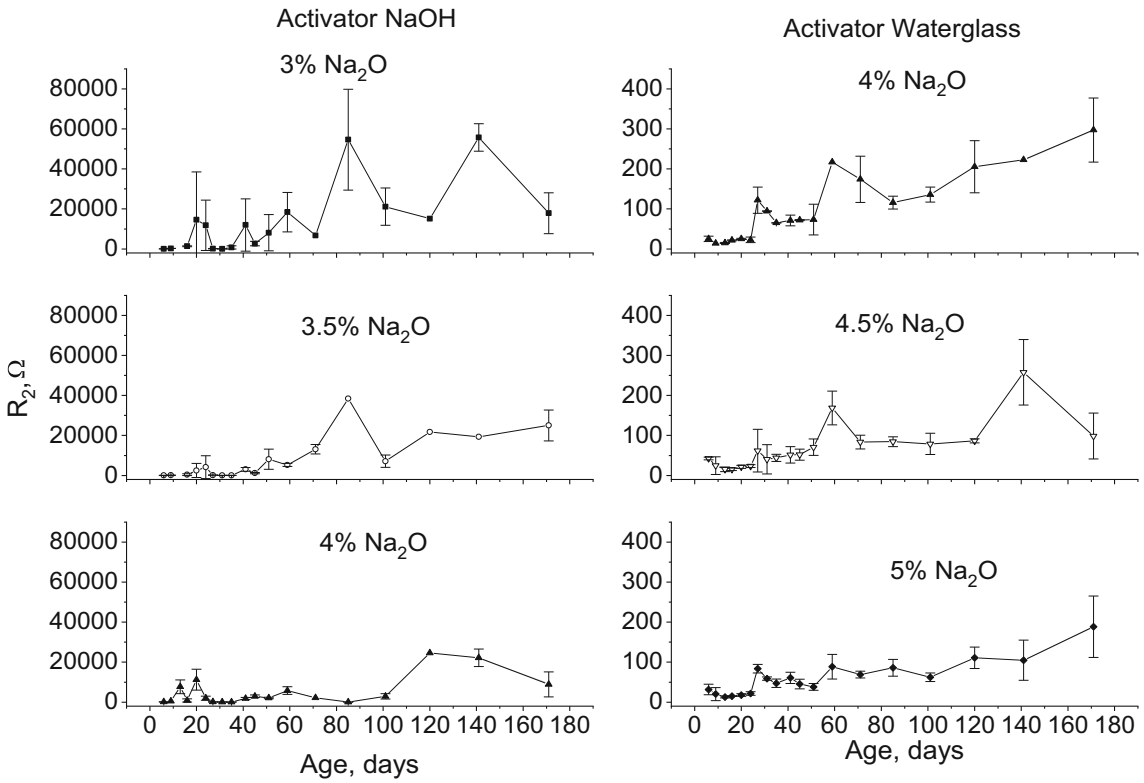

Fig. 9 Time evolution of the resistance R_2 as a function of activator and sodium oxide content

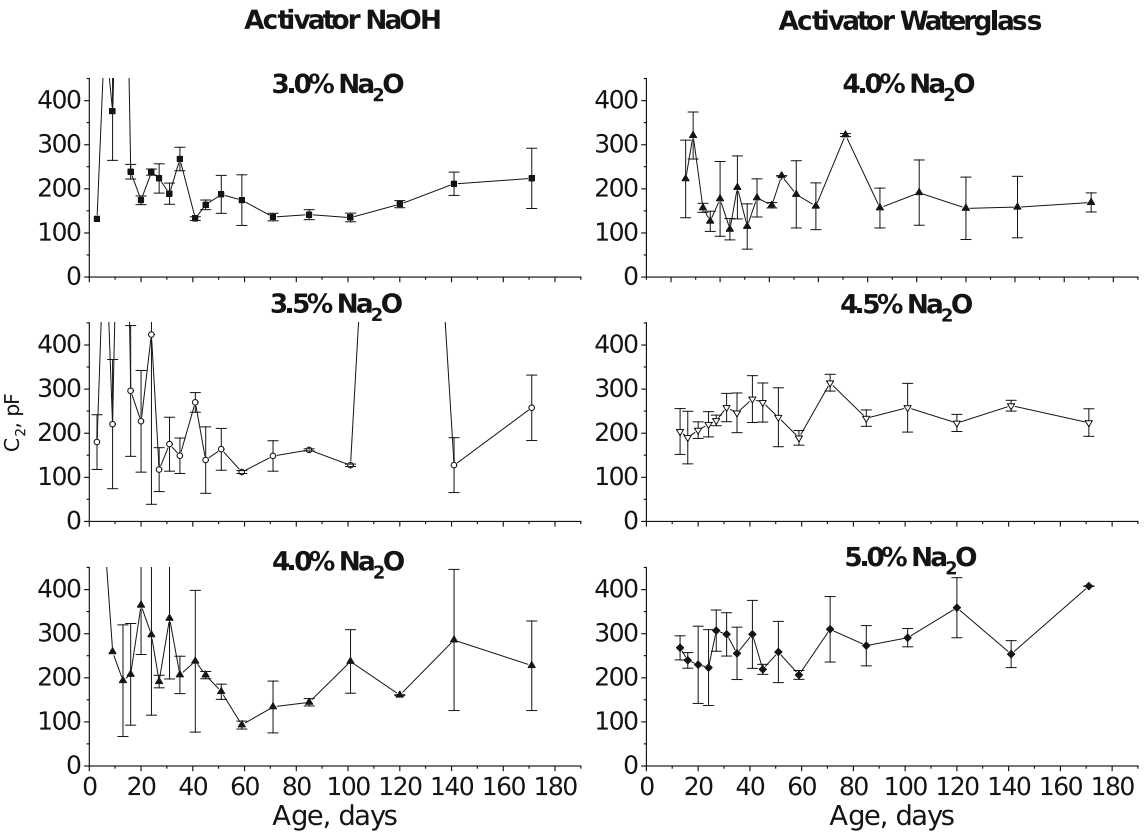

Fig. 10 Time evolution of the capacitance C_2 as a function of activator and sodium oxide content

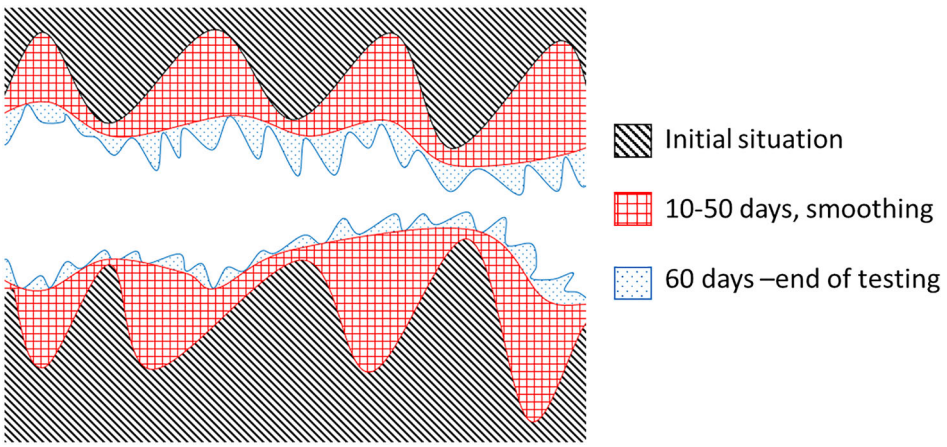

Fig. 11 Time evolution of the pore network according to the results of the capacitance C_2

90 days than from 7 to 28, possibly due to a mixed behavior according to the capacity C_2. The values of the compressive strength determined on mortars, but using the same activating solutions and precursor [31] showed an important increase of compressive strength from 7 to 28 days, and the increase from 28 to 90 days was much lower.

Regarding the samples activated with waterglass, it has to be pointed out initially that the values obtained for the sample with 4.0% Na_2O showed similar values to those of the samples activated with NaOH. They show the lowest value of capacitance C_2, and an initial decrease up to 20 days approximately and then the value remained almost constant. On the other hand, samples with 4.5 and 5.0% of sodium oxide that show a slight but constant increase, being the sample with 5.0% of Na_2O the one that has a higher value for this capacitance. It must be reminded that these two samples showed also the lowest resistance, and that they showed shrinkage macro-cracks. All these facts are in good agreement. It had also been shown that even in case of low relative humidity [49] as well as in the case of fire events [18] the water was distributed occupying all the binder inner surface, even in the presence of shrinkage cracks [50]. The low values of the resistances, especially resistance R_1, and the visual evidence, allow us to confirm that the low resistance values are due to the presence of cracks from very early ages, almost after demolding and before cutting. The increase in the value of the capacitance C_2 means that there has been continuous formation of new solid phases in contact with the electrolyte, as it was also confirmed by the low pore sizes present in the samples that could not be measured due to the detection limit of the porosimeter available. This result is also in agreement with the evolution of the compressive strength of the samples already reported in [31], where the resistance of the samples increased constantly up to 90 days, and the samples with 5.0% Na_2O presented the highest values for the measured mechanical properties. This is just a matter of the fitting of the impedance spectra.

The solid phase is proportional to the value of the capacitance C_1, assuming that the compounds that form that solid phase are of similar nature, as it is the case. This parameter is usually determined using the non-contacting measurements, when it is possible, due not only to a higher sensitivity of these measurements for the determination of the capacitance, but because it avoids the electrode-sample interface [51] avoiding the so-called dielectric amplification factor [52, 53]. The values obtained from the measurements without contact are shown on Fig. 12.

As it can see, most of the values obtained, especially for the case of the samples activated using waterglass, are very low. It is clearly seen on Fig. 13 that for 141 days, the impedance spectra of the sample activated with sodium hydroxide has a final loop, that is closed in the high frequency region, and that makes easy the calculation of the capacitance C1; while for the sample activated with waterglass the final loop is not closed at all in the high frequency region, and the value obtained for the fitting of the capacitance C_1 could be whichever. Due to this fact the values for the capacitance C_1 have been obtained from contact measurements. It is true that the values obtained are not coincident with those obtained avoiding contact sample-electrode, but the tendency is similar, as it has been already proved [10], and for study of the tendencies it is a good approximation. Even though values may differ, due to the use of different configurations, the tendencies must be similar if the parameters really represent the evolution of the microstructure [10]. Since no impedance spectroscopy analysis has been published on this particular alkali activated material, the time evolution of the parameter C_2 is compared using contacting configuration and non-contacting setup on Fig. 14, and as it can be seen on that figure the time evolution of the capacitance has equivalent tendencies.

The importance of the frequency of the maximum of the imaginary part of the impedance (characteristic frequency) is a key value, as it is already well known, and has been used

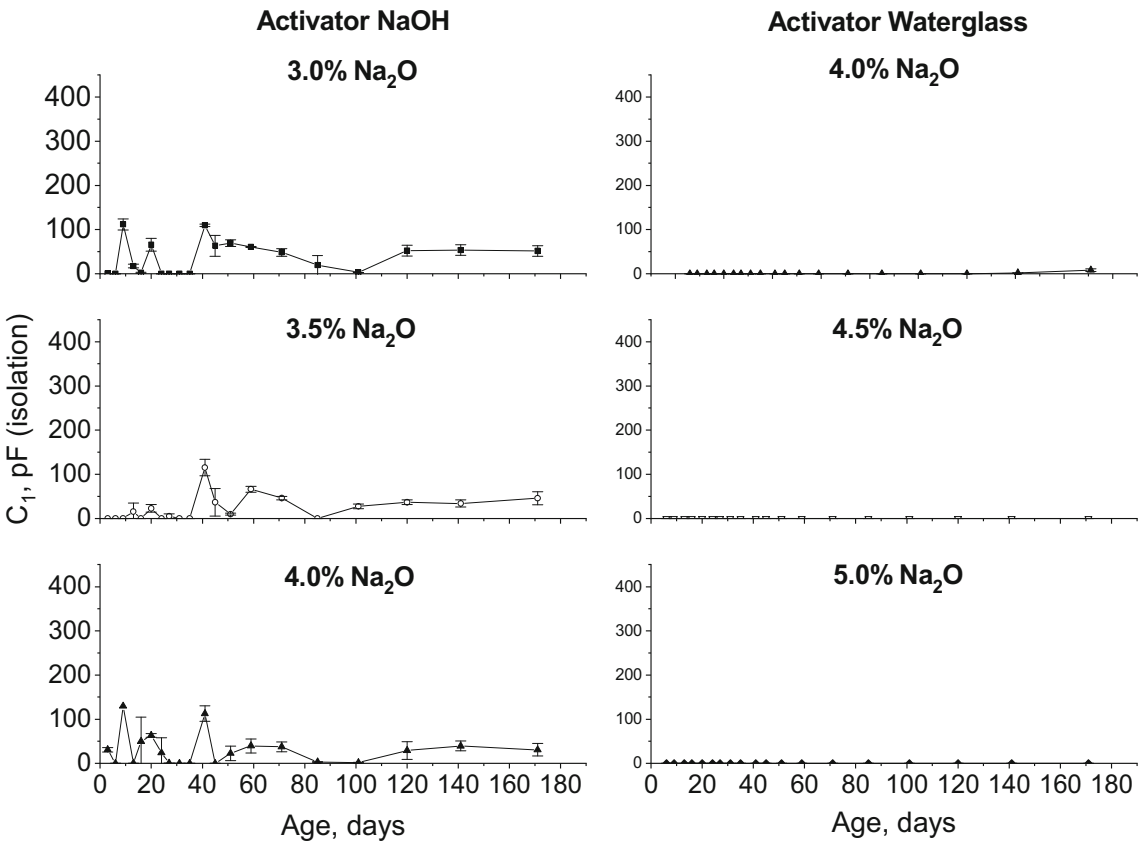

Fig. 12 Time evolution of the capacitance C_1 as a function of activator and sodium oxide content for measurements avoiding contact sample-electrode

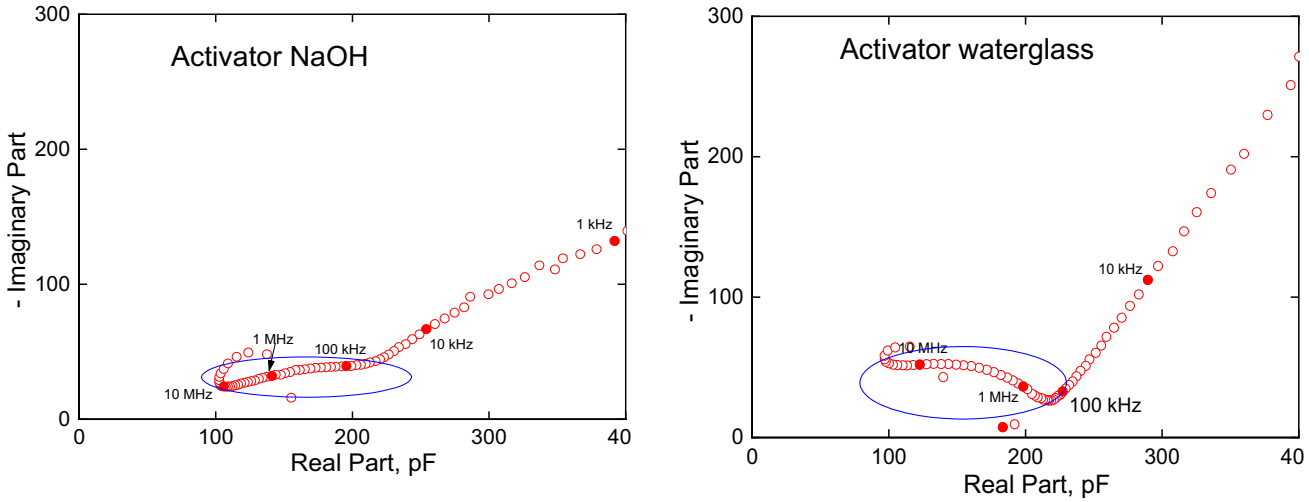

Fig. 13 Cole–Cole plot obtained at 141 days for samples activated with sodium hydroxide (left) and waterglass (right) with the maximum content of sodium oxide

for the study of the microstructural evolution of alkali activated materials [48]. In that case the loops were complete, and the value of the characteristic frequency was far from the end of the frequency range, even though the geometrical conditions were much farther from the plane condenser ideal situation than in our case. This result could be expected due to the different nature of the slag, and consequently the differences in the solids formed and their properties. The change in the characteristic frequency is the same as it was observed in [29], that is coincident with the behavior of ordinary Portland cement [33] and other cement-based materials

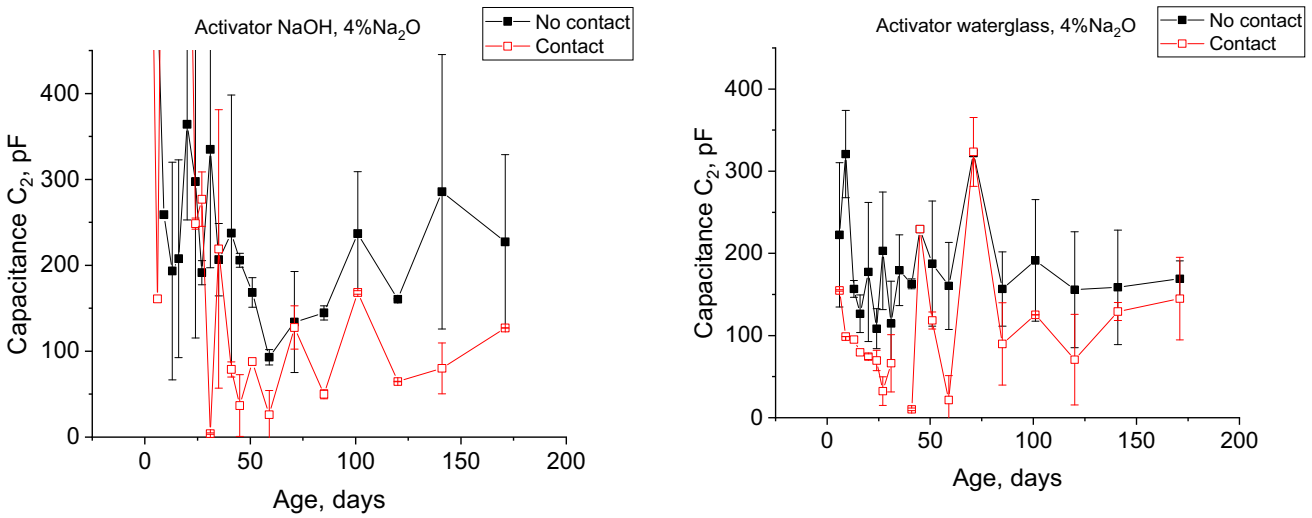

Fig. 14 Time evolution of the capacitance C_2 as a function of time and activator used for samples with 4%Na_2O, with and without contact between sample and electrodes

[54], the characteristic frequency decreases with time, closing the loop, and making more accurate the fitting of every parameter of the equivalent circuit.

As it is shown on Fig. 14 the time evolution of the electrical parameters that can be determined using both equivalent circuits is very similar. It had also been proved in the case of change in the sample thickness [10]. So, the capacitance C_1 will be studied using the contacting measurements.

The results of the capacitance C_1 obtained from the contacting setup are depicted on Fig. 15.

As it can be seen on Fig. 15, the value of the capacitance is not very different from one sample to another. This fact is coincident with the results of the thermogravimetric analysis [32], that as a general fact it can be said that the long-term value of the capacitance is higher for samples activated with waterglass. For this activator, the higher percentage of sodium oxide also causes a higher value of the capacitance.

The value of the capacitance C_1 slightly increases with time or remains constant. This fact means an increase in the solid fraction, and a decrease of the porosity as it was shown on Fig. 3. The values of the porosity of the samples obtained activating the slag with waterglass did not show this behaviour. The porosity at 7 days for the samples with 4.5 and 5.0% of sodium oxide were the smallest of all the samples. The porosity increased with time, from 7 to 28 days for both samples, while the value of the capacitance did not vary. The change in the porosity should be due to the presence of shrinkage cracks, that continue growing with time for the case of samples with 5.0% of sodium oxide up to 90 days (bare eye visible cracks, as shown on Fig. 10), but the capacitance shows a slightly increasing tendency, in coincidence with the increase of the compressive strength [31]. For the case of the samples activated with waterglass and a percentage of Na_2O of 4.5%, the value of C_1 shows a maintained increasing tendency up to 120 days, and an approximately constant value after that age. For these samples, the porosity decreases from 28 to 90 days, but it does not reach the porosity value measured at 7 days. In this case, the constant formation of solid (increase of C_1) can counteract the effect of the cracking due to expansion and that could be the cause of the similar values for the compressive strength obtained for both materials [31]. The results are in agreement with the evolution of the capacitance C_2 that showed a constant increase in the pore surface, followed by a smoothing of the pore walls due to the formation of new solids, and then a slight increase of the surface that could be either due to the formation of new solids or to the opening of microcracks by shrinkage. These microcracks might be responsible for not having a clearly higher value of the capacitance C_1 in samples activated with waterglass, since when cracks appear the solid fraction decreases.

The values of the capacitance C_1 can also be correlated to the different hydrated phases that were found by thermogravimetry [32]. The gel percentages were higher for the samples activated with waterglass, and the higher is the sodium oxide content the higher is the value of the mass loss associated to the gel (50–200 °C) (as shown on Table 3). The values of the capacitance C_1 are as in general slightly higher for the samples activated with water glass too. The time increase of the capacity C_1 can also be associated to the increase of the mass loss due to the dehydration of the gel.

The mass loss associate to the brucite, among 200 and 400 °C, does not show an important influence of the activator, only exhibits an increase with time of the percentage of this phase, and the results are shown on Table 4, where the

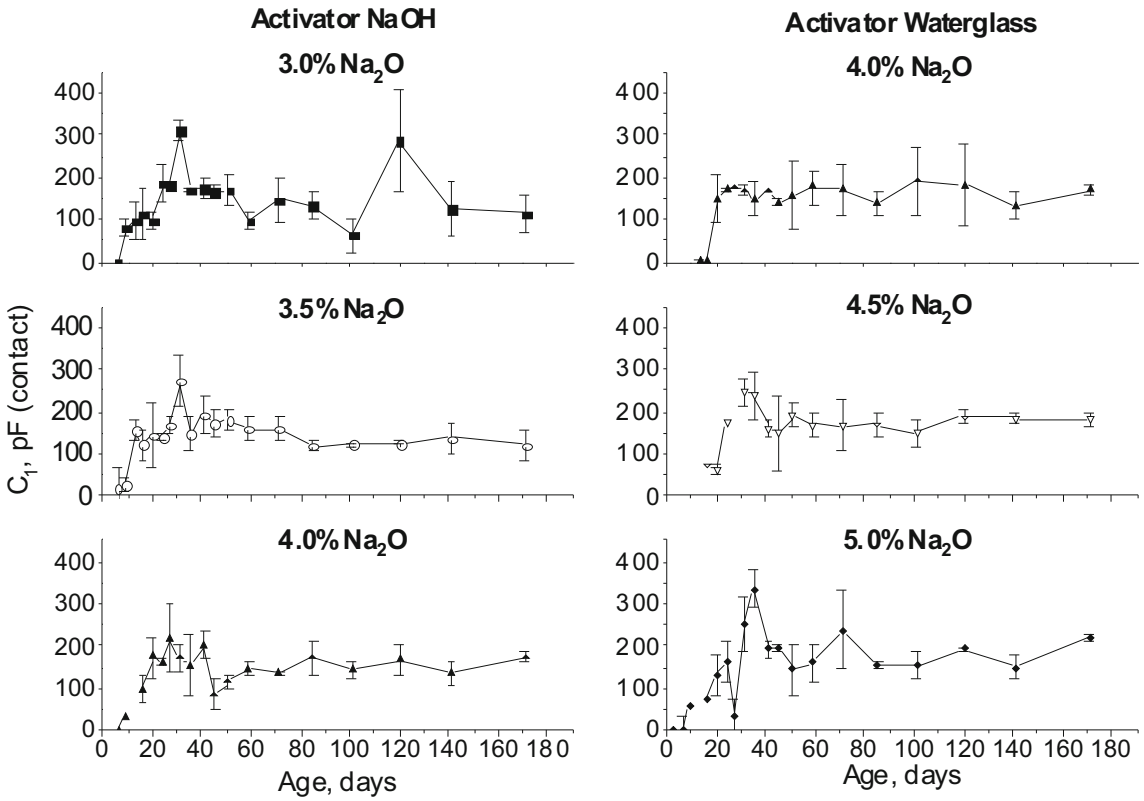

Fig. 15 Time evolution of the capacitance C_1 as a function of activator and sodium oxide content for measurements with contact sample-electrode

Table 3 Mass loss (%) associated to the gel in the thermogravimetric analysis from 50 to 200 °C

Activator	NaOH			Waterglass		
% Na_2O	3.0	3.5	4.0	4.0	4.5	5.0
7 days	4.49	5.05	5.44	5.63	5.82	6.28
28 days	5.51	6.42	6.19	6.70	8.58	8.05
90 days	6.41	6.39	8.63	10.95	10.68	11.32

Table 4 Mass loss (%) associated to the brucite in the thermogravimetric analysis from 200 to 400 °C

Activator	NaOH			Waterglass		
% Na_2O	3.0	3.5	4.0	4.0	4.5	5.0
7 days	2.44	2.65	2.86	2.35	2.58	2.43
28 days	2.76	3.09	3.14	2.85	4.38	3.11
90 days	2.50	2.81	3.44	2.54	2.62	3.12

Table 5 Mass loss (%) associated to the dehydration of the spinel in the thermogravimetric analysis from 400 to 600 °C

Activator	NaOH			Waterglass		
% Na_2O	3.0	3.5	4.0	4.0	4.5	5.0
7 days	1.84	1.60	1.73	1.25	1.31	1.11
28 days	2.35	1.64	1.97	2.46	2.34	2.03
90 days	3.47	3.36	1.82	1.68	2.16	2.29

Table 6 Mass loss (%) associated to the decarbonation in the thermogravimetric analysis from 600 to 700 °C

Activator	NaOH			Waterglass		
% Na_2O	3.0	3.5	4.0	4.0	4.5	5.0
7 days	0.56	0.60	0.65	0.27	0.42	0.50
28 days	0.65	0.58	0.63	0.70	0.56	0.27
90 days	0.67	0.73	0.51	0.25	0.25	0.25

percentage of mass lost in the range from 200 to 400 °C is shown. The same conclusion can be obtained for the dehydration of the spinel (400–600 °C), as shown on Table 5 The decarbonation that takes place among 600 and 700 °C has a behavior different from the showed for the gel, the samples activated with NaOH show a higher content of carbonates, but the differences are much smaller than for the dehydration among 50 and 200 °C and it cannot compensate those differences. The results of the mass loss during the decarbonation of the samples are shown on Table 6.

The chemical composition seems to be too similar among samples as to cause an effect on the dielectrical properties of the solids [32]. The properties have not been analysed in the other paper that uses impedance spectroscopy to analyse the microstructure of another alkali activated material [29], but from the point of view of the authors the analysis of this element is essential for understanding the development of the microstructure of porous materials [1–3], or in more recent works including supplementary cementing materials [13, 54].

4 Conclusions

According to the materials studied and the results presented the following conclusions can be reached:

- Impedance spectroscopy can be used for the microstructural characterization of alkali activated SiMn slag, using the same equivalent circuits as for standard cement based materials due to the number of time constants in each spectrum.
- The resistivity of the samples has been proved not to be suitable as a single parameter to identify the evolution of the microstructure and the mechanical properties of the materials used on this paper. The presence of shrinkage causes an important disagreement among electrical resistivity and compressive strength.
- Shrinkage causes a displacement of the frequency of the maximum of the high frequency loop, especially using non-contacting measurements, and as a consequence the capacitance associated to the solid phase has to be calculated from contacting measurements
- The capacitances show a continuous formation of solid phases, with a higher amount of solids in the case of using waterglass as activator, in agreement with other microstructural tests, and the mechanical behavior of the alkali activated SiMn slags.
- The combination of capacitances and resistances calculated from the equivalent circuit used for the fitting of the impedance spectroscopy measurements can be used to understand the mechanical behavior of the slags activated either with NaOH or waterglass. The mercury porosimetry, or the SEM analysis could not predict the mechanical behaviour, even taking the shrinkage into account. This phenomenon can also be predicted by the low resistance values obtained in the samples activated with waterglass, while the capacitance values show a continuous increase, both of the solid-solution interphase, and the solids formed.

Acknowledgements The authors wish to thank the Spanish Ministry of Science and Innovation for project funding (PID2020-118322RB-I00) through the "Programa Estatal de I+D+i Orientada a los Retos de la Sociedad" included in the "Plan Estatal de Investigación Científica y Técnica y de Innovación 2017-2020". The authors also wish to thank Cristina Rodríguez from Ferroglobe, for the supply of SiMn slag necessary to carry out this research.

Author Contributions RN: Investigation, Resources, Writing—Review & Editing. EZ Conceptualization, Writing—Review & Editing, Supervision. EGA: Conceptualization, Writing—Review & Editing, IS: Methodology, Investigation, Writing—Original Draft, Visualization.

Funding Open Access funding provided thanks to the CRUE-CSIC agreement with Springer Nature. The paper is founded by the research project granted by the Spanish Ministry of Science and Innovation for project funding (PID2020-118322RB-I00) through the "Programa Estatal de I + D + i Orientada a los Retos de la Sociedad" included in the "Plan Estatal de Investigación Científica y Técnica y de Innovación 2017–2020".

Data Availability The datasets generated during and/or analysed during the current study are available from the corresponding author on reasonable request.

Declarations

Competing Interests The authors disclose any interests directly or indirectly related to the work submitted for publication.

Ethical Approval and Consent to Participate The paper has not been submitted simultaneously to any other journal. The paper has not been published previously and includes an original work from the authors. All the data included in the work have been obtained from the fitting of experimental measurements without manipulation. No data, text, or theories by others are presented in the paper as if they were the author's own. All the authors have reviewed the final version of the manuscript and consent to participate on the publication

Consent for Publication All authors have agreed with the content and that all gave explicit consent to submit. The University of Alicante allows the publication of any paper.

References

1. Guerrero, A., Goñi, S., Macías, A., Luxán, M.P.: Effect of the starting fly ash on the microstructure and mechanical properties of fly ash-belite cement mortars. Cem. Concr. Res. **30**, 553–559 (2000). https://doi.org/10.1016/S0008-8846(00)00198-8
2. Bouguerra, A., Ledhem, A., Barquin, F., Dheilly, R.M., Queneudec, M.: Effect of microstructure on the mechanical and thermal properties of lightwight concrete prepared from clay, cement, and wood aggregates. Cem. Concr. Res. **28**, 1179–1190 (1998). https://doi.org/10.1016/S0008-8846(98)00075-1
3. Ortega, J.M., Sánchez, I., Antón, C., de Vera, G., Climent, M.A.: Influence of environment on durability of fly ash cement mortars. ACI Mater. J. **109**, 647–656 (2012)
4. Robens, E., Benzler, B., Büchel, G., Reichert, H., Schumacher, K.: Investigation of characterizing methods for the microstructure of cement. Cem. Concr. Res. **32**, 87–90 (2002). https://doi.org/10.1016/S0008-8846(01)00633-0
5. Christensen, B.J., Coverdale, R.T., Olson, R.A., Ford, S.J., Garboczi, E.J., Jennings, H.M., Mason, T.O.: Impedance spectroscopy of hydrating cement-based materials: measurement, interpretation, and application. JACerS. **77**, 2789–2804 (1994). https://doi.org/10.1111/j.1151-2916.1994.tb04507.x
6. Coverdale, R.T., Christensen, B.J., Mason, T.O., Jennings, H.M., Garboczi, E.J.: Interpretation of the impedance spectroscopy of cement paste via computer modelling. Part II dielectric response. J. Mater. Sci. **29**, 4984–4992 (1994). https://doi.org/10.1007/BF01151088
7. Coverdale, R.T., Christensen, B.J., Jennings, H.M., Mason, T.O., Bentz, D.P., Garboczi, E.J.: Interpretation of impedance spectroscopy of cement paste via computer modelling. Part I Bulk conductivity and offset resistance. J. Mater. Sci. **30**, 712–719 (1995). https://doi.org/10.1007/BF00356331
8. Vladikova, D., Stoynov, Z., Ilkov, L.: Differential impedance analysis on single crystal and polycrystalline Yttrium Iron Garnets. Pol. J. Chem. **71**, 1196–1203 (1997)
9. Andrade, C., Blanco, V.M., Collazo, A., Keddam, M., Noâ Voa, X.R., Takenouti, H.: Cement paste hardening process studied by impedance spectroscopy. Electrochim. Acta. **44**, 4313–4318 (1999). https://doi.org/10.1016/S0013-4686(99)00147-4
10. Cabeza, M., Merino, P., Miranda, A., Nóvoa, X.R., Sanchez, I.: Impedance spectroscopy study of hardened Portland cement paste. Cem. Concr. Res. **32**, 881–891 (2002). https://doi.org/10.1016/S0008-8846(02)00720-2
11. Cruz, J.M., Payá, J., Lalinde, L.F., Fita, I.C.: Evaluación de las propiedades eléctricas de morteros de cemento con puzolanas. Mater. Construcción. **61**, 7–26 (2011). https://doi.org/10.3989/mc.2010.53709
12. Cruz, J.M., Fita, I.C., Soriano, L., Payá, J., Borrachero, M.V.: The use of electrical impedance spectroscopy for monitoring the hydration products of Portland cement mortars with high percentage of pozzolans. Cem. Concr. Res. **50**, 51–61 (2013). https://doi.org/10.1016/j.cemconres.2013.03.019
13. Ortega, J.M., Sánchez, I., Climent, M.A.: Impedance spectroscopy study of the effect of environmental conditions in the microstructure development of OPC and slag cement mortars. Arch. Civ. Mech. Eng. **15**, 569–583 (2015). https://doi.org/10.1016/j.acme.2014.06.002
14. Jung, S.H., Saraswathy, V., Karthick, S., Kathirvel, P., Kwon, S.J.: Microstructure characteristics of fly ash concrete with rice husk ash and lime stone powder. Int. J. Concr. Struct. Mater. **12**, 1–9 (2018). https://doi.org/10.1186/s40069-018-0257-4
15. Cabeza, M., Merino, P., Nóvoa, X.R., Sánchez, I.: Electrical effects generated by mechanical loading of hardened Portland cement paste. Cem. Concr. Compos. **25**, 351–356 (2003). https://doi.org/10.1016/S0958-9465(02)00053-7
16. Li, Y., Sui, C.E., Ding, Q.J.: Study on the cracking process of cement-based materials by AC impedance method and ultrasonic method. J. Nondestruct. Eval. **31**, 284–291 (2012). https://doi.org/10.1007/s10921-012-0142-z
17. Sánchez, I., López, M.P., Ortega, J.M., Climent, M.Á.: Impedance spectroscopy: an efficient tool to determine the non-steady-state chloride diffusion coefficient in building materials. Mater. Corros. **62**, 139–145 (2011). https://doi.org/10.1002/maco.201005775
18. Sánchez, I., Sánchez, M., Climent, M.A., Alonso, M.C.: Impedance spectroscopy to characterise microsctructural changes in liquid and solid phases of mortars exposed to high temperatura. In: E.A.B.K., Dehn, F. (ed.) 2nd Int. RILEM Work. Concr. Spalling Due to Fire Expo., RILEM Publications SARL, Delft, pp. 43–51 (2011). http://rilem.net/gene/main.php?base=500218&id_publication=408&id_papier=7665. Accessed 14 Dec 2015.
19. Sedaghatdoost, A., Behfarnia, K., Moosaei, H., Bayati, M., Vaezi, M.S.: Investigation on the mechanical properties and microstructure of eco-friendly mortar containing WGP at elevated temperature. Int. J. Concr. Struct. Mater. **15**, 1–9 (2021). https://doi.org/10.1186/s40069-020-00434-9
20. White, C.E., Olds, D.P., Hartl, M., Hjelm, R.P., Page, K.: Evolution of the pore structure during the early stages of the alkali-activation reaction: an in situ small-angle neutron scattering investigation. J. Appl. Crystallogr. **50**, 61–75 (2017). https://doi.org/10.1107/S1600576716018331
21. Hanjitsuwan, S., Hunpratub, S., Thongbai, P., Maensiri, S., Sata, V., Chindaprasirt, P.: Effects of NaOH concentrations on physical and electrical properties of high calcium fly ash geopolymer paste. Cem. Concr. Compos. **45**, 9–14 (2014). https://doi.org/10.1016/j.cemconcomp.2013.09.012
22. Park, J.H., Park, C., Joh, S.H., Lee, H.S.: Effect of curing condition on resistance to chloride ingress in concrete using ground granulated blast furnace slag. Materials **12**, 3233 (2019). https://doi.org/10.3390/ma12193233

23. Zhang, L., Niu, D., Wen, B., Fu, Q., Zhang, Y.: Corrosion rate models of reinforcement in modified coral aggregate concrete. Constr. Build. Mater. **288**, 123099 (2021). https://doi.org/10.1016/j.conbuildmat.2021.123099
24. Zhao, K., Liang, Y., Ji, T., Lu, Y., Lin, X.: Effect of activator types and concentration of CO_2 on the steel corrosion in the carbonated alkali-activated slag concrete. Constr. Build. Mater. **262**, 120044 (2020). https://doi.org/10.1016/j.conbuildmat.2020.120044
25. Shi, J., Wu, M., Ming, J.: Long-term corrosion resistance of reinforcing steel in alkali-activated slag mortar after exposure to marine environments. Corros. Sci. **179**, 109175 (2021). https://doi.org/10.1016/j.corsci.2020.109175
26. Zmeskal, O., Trhlikova, L., Pospisil, J., Fiala, L., Florian, P.: Investigation of electric and thermal properties of alkali-activated aluminosilicates with a cnt admixture. Ceramics **64**, 180–189 (2020). https://doi.org/10.13168/cs.2020.0007
27. Rovnaník, P., Kusák, I., Bayer, P., Schmid, P., Fiala, L.: Comparison of electrical and self-sensing properties of Portland cement and alkali-activated slag mortars. Cem. Concr. Res. **118**, 84–91 (2019). https://doi.org/10.1016/j.cemconres.2019.02.009
28. Kim, M.K., Le, H.V., Kim, D.J.: Electromechanical response of smart ultra-high performance concrete under external loads corresponding to different electrical measurements. Sensors **21**, 1–19 (2021). https://doi.org/10.3390/s21041281
29. Hu, X., Shi, C., Liu, X., Zhang, Z.: Studying the effect of alkali dosage on microstructure development of alkali-activated slag pastes by electrical impedance spectroscopy (EIS). Constr. Build. Mater. **261**, 119982 (2020). https://doi.org/10.1016/j.conbuildmat.2020.119982
30. Navarro, R., Zornoza, E., Garcés, P., Sánchez, I., Alcocel, E.G.: Optimization of the alkali activation conditions of ground granulated SiMn slag. Constr. Build. Mater. **150**, 781–791 (2017). https://doi.org/10.1016/j.conbuildmat.2017.06.064
31. Navarro, R., Alcocel, E.G., Sánchez, I., Garcés, P., Zornoza, E.: Mechanical properties of alkali activated ground SiMn slag mortars with different types of aggregates. Constr. Build. Mater. **186**, 79–89 (2018). https://doi.org/10.1016/j.conbuildmat.2018.07.093
32. Navarro, R., García-Alcocel, E., Sánchez, I., Zornoza, E.: Influence of the type and concentration of activator on the microstructure of alkali activated SiMn Slag pastes. Constr. Build. Mater. (2022). https://doi.org/10.1016/j.conbuildmat.2022.128067
33. Cabeza, M., Keddam, M., Nóvoa, X.R., Sánchez, I., Takenouti, H.: Impedance spectroscopy to characterize the pore structure during the hardening process of Portland cement paste. Electrochim. Acta. **51**, 1831–1841 (2006). https://doi.org/10.1016/j.electacta.2005.02.125
34. Pastor, J.L., Ortega, J.M., Flor, M., López, M.P., Sánchez, I., Climent, M.A.: Microstructure and durability of fly ash cement grouts for micropiles. Constr. Build. Mater. **117**, 154 (2016). https://doi.org/10.1016/j.conbuildmat.2016.04.154
35. UNE 80225:2012. Methods of testing cement. Chemical analysis. Determination of reactive SiO_2 content in cements, puzzolanas and fly ash (2012)
36. UNE 196-2:2014. Method of testing cement. Part 2: Chemical analysis of cement (2014)
37. UNE-EN ISO 17892-3:2018 Geotechnical investigation and testing—Laboratory testing of soil—Part 3: Determination of particle density (2018)
38. Navarro, R., Alcocel, E.G., Sánchez, I., Garcés, P., Zornoza, E.: Corrosion resistance of steel reinforcements embedded in alkali activated ground granulated SiMn slag mortars. Constr. Build. Mater. **230**, 116917 (2020). https://doi.org/10.1016/j.conbuildmat.2019.116917
39. UNE-EN 196-3:2017. Methods of testing cement—Part 3. Determination of setting times and soundness (2017)
40. Barsoukov, E., McDonald, J.R.: Impedance Spectroscopy Theory, Experiment, and Applications. Wiley-Interscience, Hoboken (2005)
41. Stoynov, Z.: Differential impedance analysis—an insight into the experimental data. Pol. J. Chem. **71**, 1204–1210 (1997)
42. Vladikova, D., Stoynov, Z., Viviani, M.: Application of the differential impedance analysis for investigation of electroceramics. J. Eur. Ceram. Soc. **24**, 1121–1127 (2004). https://doi.org/10.1016/S0955-2219(03)00585-5
43. Sánchez, I., Antón, C., de Vera, G., Ortega, J.M., Climent, M.A.: Moisture distribution in partially saturated concrete studied by impedance spectroscopy. J. Nondestruct. Eval. **32**, 362–371 (2013). https://doi.org/10.1007/s10921-013-0190-z
44. Shi, Z., Shi, C., Wan, S., Ou, Z.: Effect of alkali dosage on alkali-silica reaction in sodium hydroxide activated slag mortars. Constr. Build. Mater. **143**, 16–23 (2017). https://doi.org/10.1016/j.conbuildmat.2017.03.125
45. Li, Z., Liang, X., Liu, C., Liang, M., van Breugel, K., Ye, G.: Thermal deformation and stress of alkali-activated slag concrete under semi-adiabatic condition: experiments and simulations. Cem. Concr. Res. **159**, 106887 (2022). https://doi.org/10.1016/j.cemconres.2022.106887
46. Gao, X., Yao, X., Wang, C., Geng, C., Yang, T.: Properties and microstructure of eco-friendly alkali-activated slag cements under hydrothermal conditions relevant to well cementing applications. Constr. Build. Mater. **318**, 125973 (2022). https://doi.org/10.1016/j.conbuildmat.2021.125973
47. Sánchez, I., Nóvoa, X.R., de Vera, G., Climent, M.A.: Microstructural modifications in Portland cement concrete due to forced ionic migration tests. Study by impedance spectroscopy. Cem. Concr. Res. **38**, 1015–1025 (2008). https://doi.org/10.1016/j.cemconres.2008.03.012
48. Nath, S.K., Kumar, S.: Reaction kinetics, microstructure and strength behavior of alkali activated silico-manganese (SiMn) slag—fly ash blends. Constr. Build. Mater. **147**, 371–379 (2017). https://doi.org/10.1016/j.conbuildmat.2017.04.174
49. Antón, C., Climent, M.A., de Vera, G., Sánchez, I., Andrade, C.: An improved procedure for obtaining and maintaining well characterized partial water saturation states on concrete samples to be used for mass transport tests. Mater. Struct. **46**, 1389–1400 (2012). https://doi.org/10.1617/s11527-012-9981-4
50. Ortega, J.M., Sánchez, I., Climent, M.Á.: Influence of different curing conditions on the pore structure and the early age properties of mortars with fly ash and blast-furnace slag. Mater. Constr. **63**, 219–234 (2013). https://doi.org/10.3989/mc.2012.06111
51. Andrade, C., Blanco, V.M., Collazo, A., Keddam, M., Noâ Voa, X.R., Takenouti, H.: Cement paste hardening process studied by impedance spectroscopy. Electrochim. Acta. **44**, 4313–4318 (1999)
52. Christensen, B.J., Coverdale, T., Olson, R.A., Ford, S.J., Garboczi, E.J., Jennings, H.M., Mason, T.O.: Impedance spectroscopy of hydrating cement-based materials: measurement, interpretation, and application. J. Am. Ceram. Soc. **77**, 2789–2804 (1994). https://doi.org/10.1111/j.1151-2916.1994.tb04507.x
53. Coverdale, R.T., Christensen, B.J., Mason, T.O., Jennings, H.M., Garboczi, E.J.: Interpretation of the impedance spectroscopy of cement paste via computer modelling—Part II Dielectric response. J. Mater. Sci. **29**, 4984–4992 (1994). https://doi.org/10.1007/BF01151088

54. Ortega, J.M., Letelier, V., Solas, C., Moriconi, G., Climent, M.Á., Sánchez, I.: Long-term effects of waste brick powder addition in the microstructure and service properties of mortars. Constr. Build. Mater. **182**, 691–702 (2018). https://doi.org/10.1016/j.conbuildmat.2018.06.161